iScience, Volume *24*

Supplemental information

Proteostasis regulated by testis-specific ribosomal protein RPL39L maintains mouse spermatogenesis

Qianxing Zou, Lele Yang, Ruona Shi, Yuling Qi, Xiaofei Zhang, and Huayu Qi

SUPPLEMENTAL INFORMATION

Proteostasis regulated by testis-specific ribosomal protein RPL39L maintains mouse spermatogenesis

Qianxing Zou, Lele Yang, Ruona Shi, Yuling Qi, Xiaofei Zhang, Huayu Qi

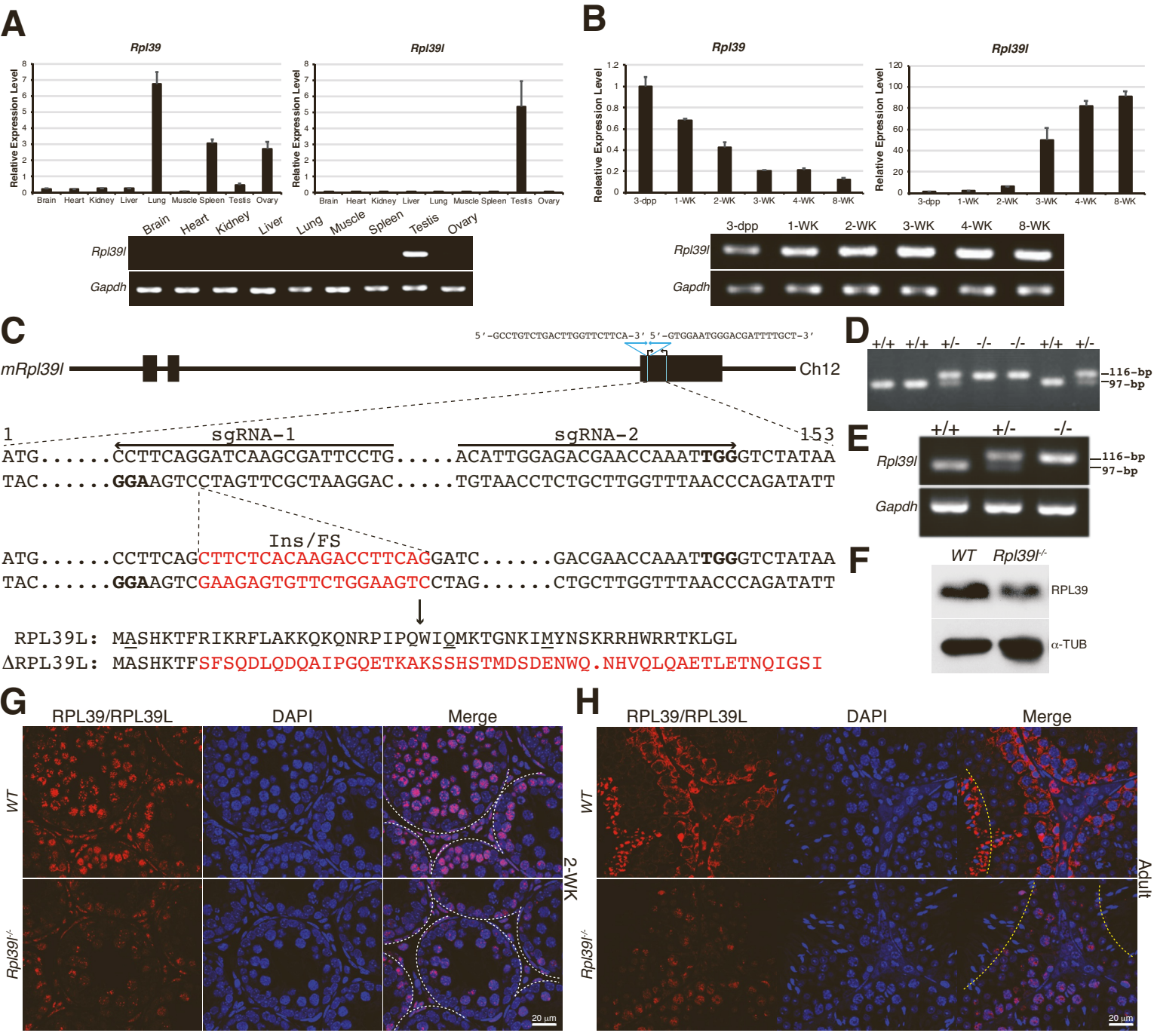
A
Rpl39
Rpl39l
Relative Expression Level
Brain Heart Kidney Liver Lung Muscle Spleen Testis Ovary
Rpl39l
Gapdh
B
Rpl39
Rpl39l
Releative Expression Level
3-dpp 1-WK 2-WK 3-WK 4-WK 8-WK
C
mRpl39l
Ch12
5′-GCCTGTCTGACTTGGTTCTTCA-3′ 5′-GTGGAATGGGACGATTTTGCT-3′
1
153
sgRNA-1
sgRNA-2
ATG.....CCTTCAGGATCAAGCGATTCCTG.....ACATTGGAGACGAACCAAATTGGGTCTATAA
TAC.....GGAAGTCCTAGTTCGCTAAGGAC.....TGTAACCTCTGCTTGGTTTAACCCAGATATT
Ins/FS
ATG.....CCTTCAGCTTCTCACAAGACCTTCAGGATC.....GACGAACCAAATTGGGTCTATAA
TAC.....GGAAGTCGAAGAGTGTTCTGGAAGTCCTAG.....CTGCTTGGTTTAACCCAGATATT
RPL39L: MASHKTFRIKRFLAKKQKQNRPIPQWIQMKTGNKIMYNSKRRHWRRTKLGL
ΔRPL39L: MASHKTFSFSQDLQDQAIPGQETKAKSSHSTMDSDENWQ.NHVQLQAETLETNQIGSI
D
+/+ +/+ +/- -/- -/- +/+ +/-
116-bp
97-bp
E
+/+ +/- -/-
Rpl39l
Gapdh
116-bp
97-bp
F
WT Rpl39l-/-
RPL39
α-TUB
G
RPL39/RPL39L
DAPI
Merge
WT
Rpl39l-/-
2-WK
20 μm
H
RPL39/RPL39L
DAPI
Merge
WT
Rpl39l-/-
Adult
20 μm

Figure S1

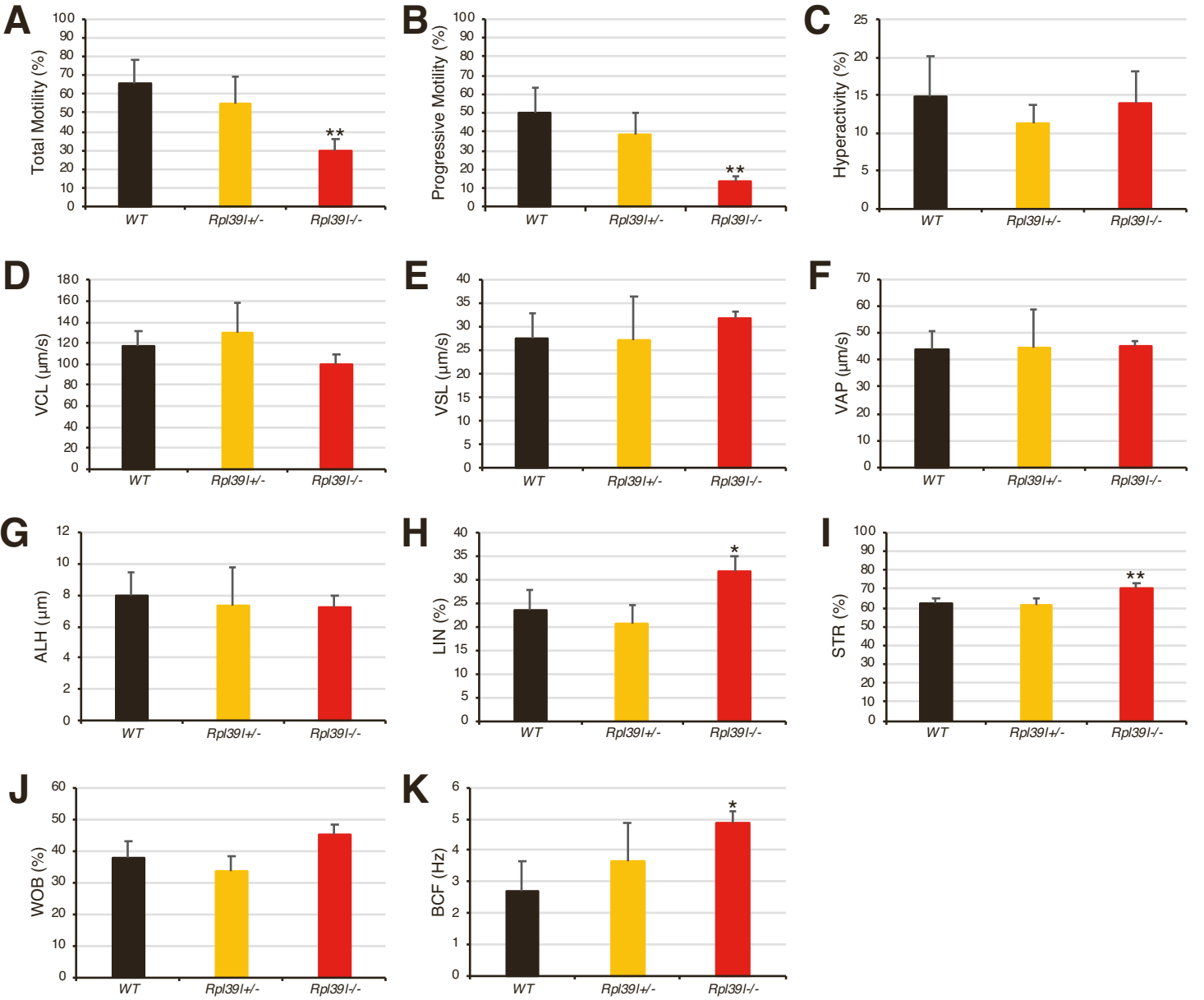
A
Total Motility (%)
100
90
80
70
60
50
40
30
20
10
0
**
WT
Rpl39l+/-
Rpl39l-/-
B
Progressive Motility (%)
100
90
80
70
60
50
40
30
20
10
0
**
WT
Rpl39l+/-
Rpl39l-/-
C
Hyperactivity (%)
25
20
15
10
5
0
WT
Rpl39l+/-
Rpl39l-/-
D
VCL (µm/s)
180
160
140
120
100
80
60
40
20
0
WT
Rpl39l+/-
Rpl39l-/-
E
VSL (µm/s)
40
35
30
25
20
15
10
5
0
WT
Rpl39l+/-
Rpl39l-/-
F
VAP (µm/s)
70
60
50
40
30
20
10
0
WT
Rpl39l+/-
Rpl39l-/-
G
ALH (µm)
12
10
8
6
4
2
0
WT
Rpl39l+/-
Rpl39l-/-
H
LIN (%)
40
35
30
25
20
15
10
5
0
*
WT
Rpl39l+/-
Rpl39l-/-
I
STR (%)
100
90
80
70
60
50
40
30
20
10
0
**
WT
Rpl39l+/-
Rpl39l-/-
J
WOB (%)
60
50
40
30
20
10
0
WT
Rpl39l+/-
Rpl39l-/-
K
BCF (Hz)
6
5
4
3
2
1
0
*
WT
Rpl39l+/-
Rpl39l-/-

Figure S2

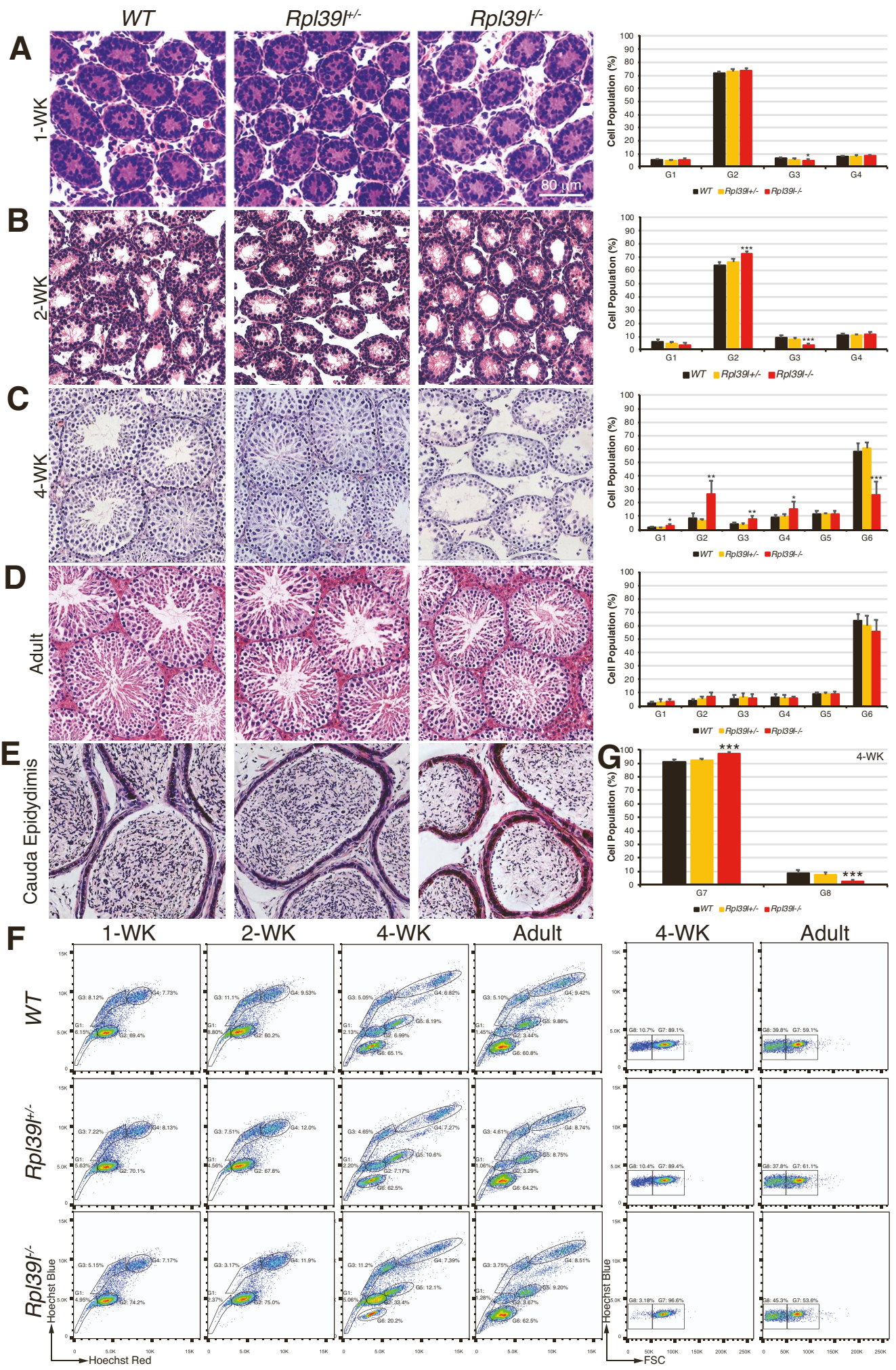
WT
Rpl39l+/-
Rpl39l-/-
A
1-WK
80 μm
B
2-WK
C
4-WK
D
Adult
E
Cauda Epidydimis
Cell Population (%)
G1
G2
G3
G4
G5
G6
WT
Rpl39l+/-
Rpl39l-/-
G
4-WK
G7
G8
F
1-WK
2-WK
4-WK
Adult
Hoechst Blue
Hoechst Red
FSC

Figure S3

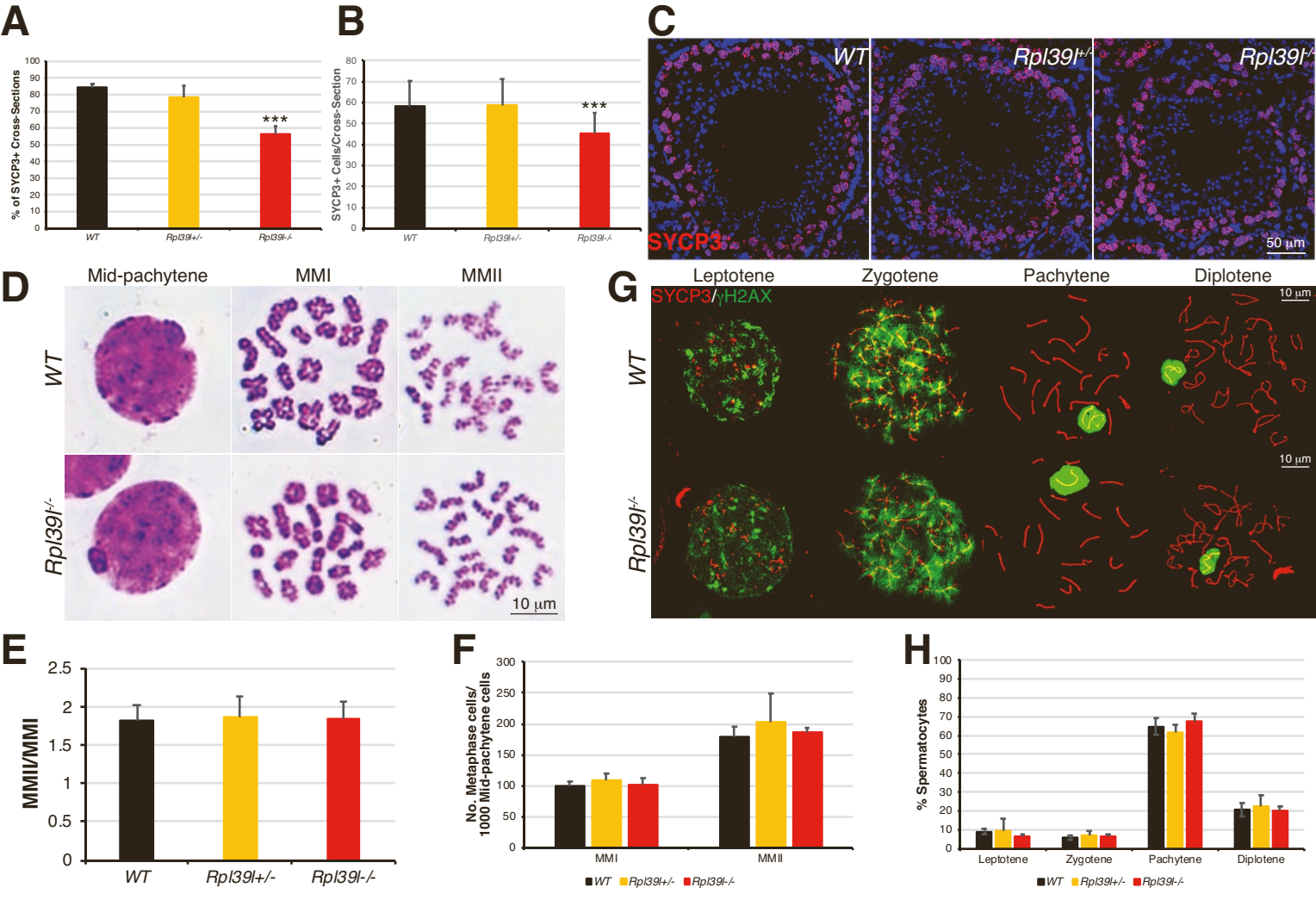
A
% of SYCP3+ Cross-Sections
100
90
80
70
60
50
40
30
20
10
0
***
WT
Rpl39l+/-
Rpl39l-/-
B
SYCP3+ Cells/Cross-Section
80
70
60
50
40
30
20
10
0
***
WT
Rpl39l+/-
Rpl39l-/-
C
WT
Rpl39l+/-
Rpl39l-/-
SYCP3
50 µm
D
Mid-pachytene
MMI
MMII
WT
Rpl39l-/-
10 µm
G
Leptotene
Zygotene
Pachytene
Diplotene
SYCP3/γH2AX
WT
Rpl39l-/-
10 µm
10 µm
E
MMII/MMI
2.5
2
1.5
1
0.5
0
WT
Rpl39l+/-
Rpl39l-/-
F
No. Metaphase cells/ 1000 Mid-pachytene cells
300
250
200
150
100
50
0
MMI
MMII
WT
Rpl39l+/-
Rpl39l-/-
H
% Spermatocytes
100
90
80
70
60
50
40
30
20
10
0
Leptotene
Zygotene
Pachytene
Diplotene
WT
Rpl39l+/-
Rpl39l-/-

Figure S4

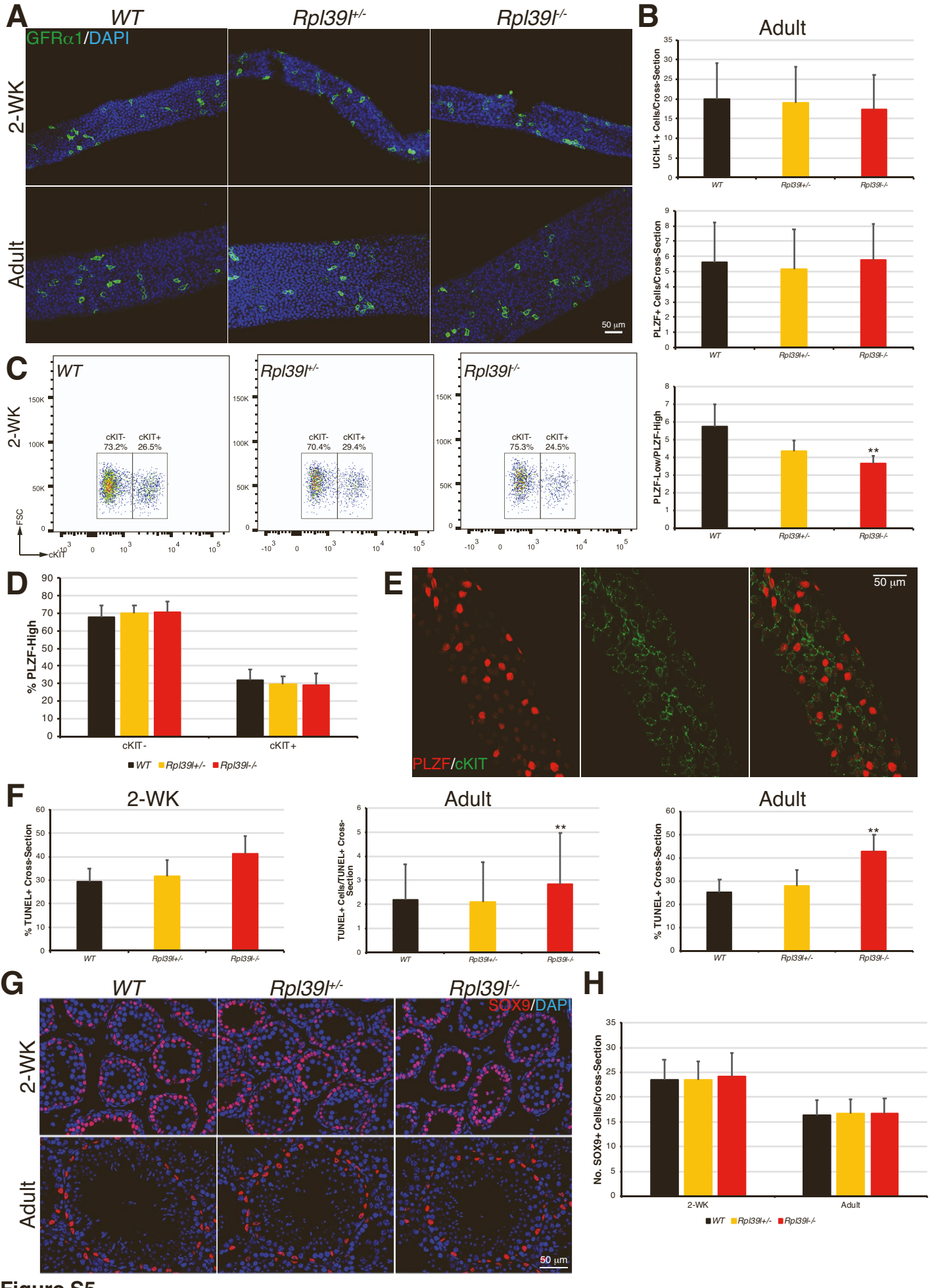
A
WT
Rpl39l+/-
Rpl39l-/-
GFRα1/DAPI
2-WK
Adult
50 μm
B
Adult
UCHL1+ Cells/Cross-Section
PLZF+ Cells/Cross-Section
PLZF-Low/PLZF-High
**
C
WT
Rpl39l+/-
Rpl39l-/-
2-WK
cKIT- 73.2%
cKIT+ 26.5%
cKIT- 70.4%
cKIT+ 29.4%
cKIT- 75.3%
cKIT+ 24.5%
FSC
cKIT
D
% PLZF-High
cKIT-
cKIT+
WT
Rpl39l+/-
Rpl39l-/-
E
PLZF/cKIT
50 μm
F
2-WK
Adult
% TUNEL+ Cross-Section
TUNEL+ Cells/TUNEL+ Cross-Section
**
G
WT
Rpl39l+/-
Rpl39l-/-
SOX9/DAPI
2-WK
Adult
50 μm
H
No. SOX9+ Cells/Cross-Section
2-WK
Adult
WT
Rpl39l+/-
Rpl39l-/-

Figure S5

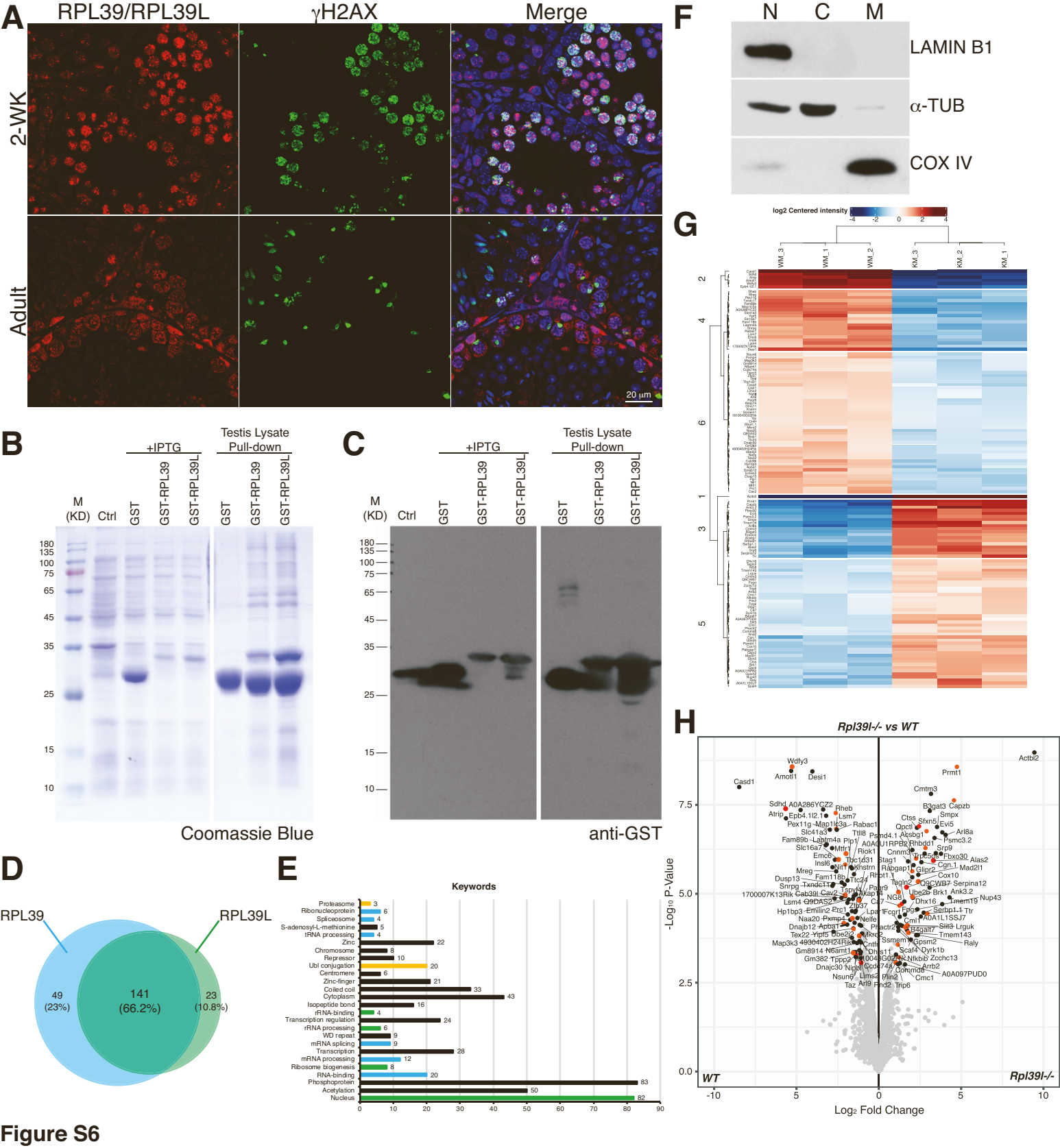
A
RPL39/RPL39L
γH2AX
Merge
2-WK
Adult
20 μm
B
+IPTG
Testis Lysate Pull-down
M (KD)
Ctrl
GST
GST-RPL39
GST-RPL39L
180
135
100
75
65
45
35
25
15
10
Coomassie Blue
C
anti-GST
D
RPL39
RPL39L
49 (23%)
141 (66.2%)
23 (10.8%)
E
Keywords
Proteasome
Ribonucleoprotein
Spliceosome
S-adenosyl-L-methionine
tRNA processing
Zinc
Chromosome
Repressor
Ubl conjugation
Centromere
Zinc-finger
Coiled coil
Cytoplasm
Isopeptide bond
rRNA-binding
Transcription regulation
rRNA processing
WD repeat
mRNA splicing
Transcription
mRNA processing
Ribosome biogenesis
RNA-binding
Phosphoprotein
Acetylation
Nucleus
F
N
C
M
LAMIN B1
α-TUB
COX IV
G
log2 Centered intensity
WM_3
WM_1
WM_2
KM_3
KM_2
KM_1
H
Rpl39l-/- vs WT
-Log10 P-Value
Log2 Fold Change
WT
Rpl39l-/-

Figure S6

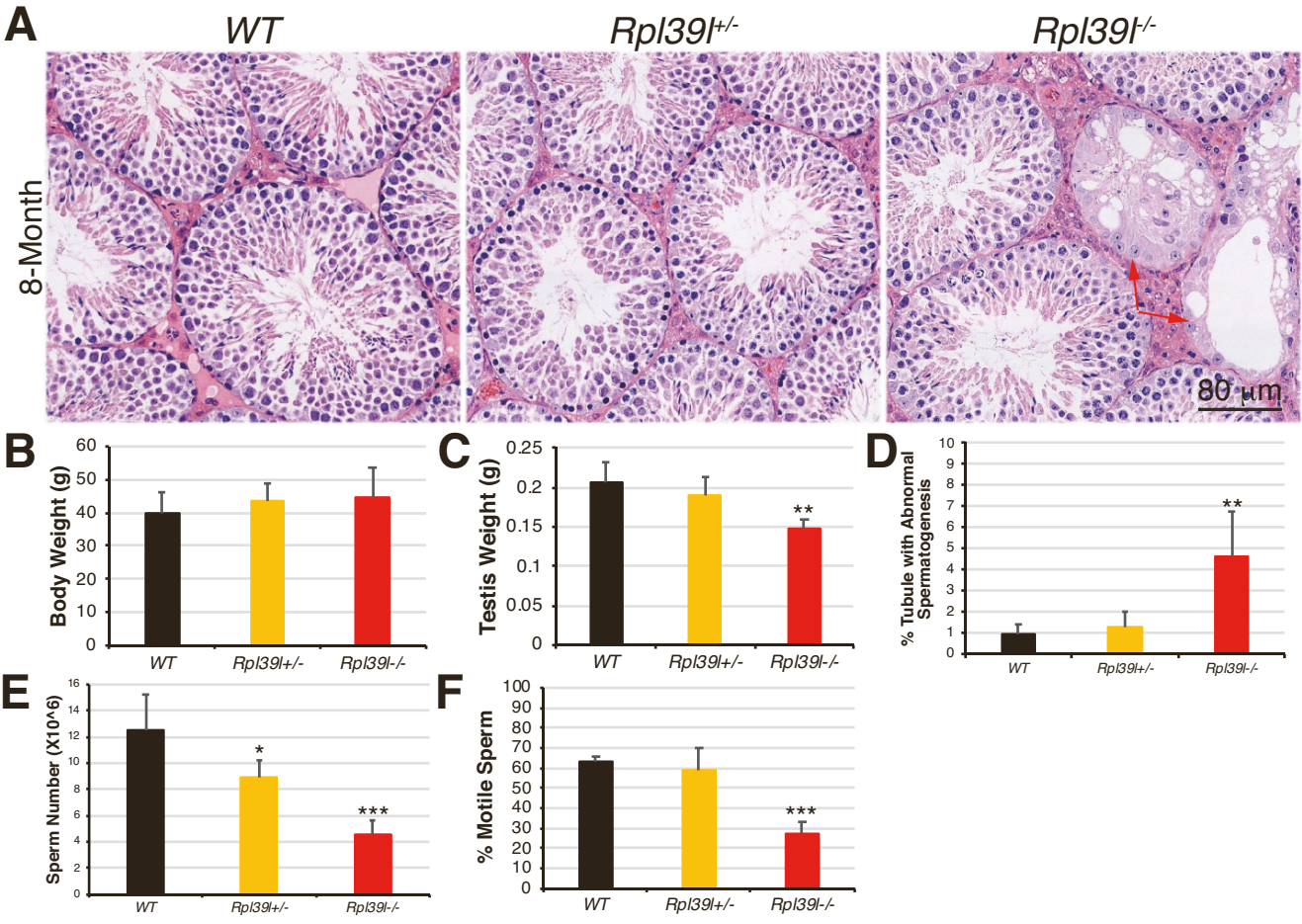
A
WT
Rpl39l+/-
Rpl39l-/-
8-Month
80 μm
B
Body Weight (g)
60
50
40
30
20
10
0
WT
Rpl39l+/-
Rpl39l-/-
C
Testis Weight (g)
0.25
0.2
0.15
0.1
0.05
0
**
WT
Rpl39l+/-
Rpl39l-/-
D
% Tubule with Abnormal Spermatogenesis
10
9
8
7
6
5
4
3
2
1
0
**
WT
Rpl39l+/-
Rpl39l-/-
E
Sperm Number (X10^6)
16
14
12
10
8
6
4
2
0
*
***
WT
Rpl39l+/-
Rpl39l-/-
F
% Motile Sperm
100
90
80
70
60
50
40
30
20
10
0
***
WT
Rpl39l+/-
Rpl39l-/-

Figure S7

SUPPLEMENTAL FIGURE LEGENDS

Figure S1: Expression of *Rpl39*/*Rpl39l* paralogs and generation of *Rpl39l* null mice. Related to Figure 1.

(A) Quantitative RT-PCR of *Rpl39* and *Rpl39l* in adult male mouse tissues. *Gapdh* was used as the control. Images of agarose gel electrophoresis of RT-PCR products are shown below.

(B) Quantitative RT-PCR of *Rpl39* and *Rpl39l* in mouse testes at various post-natal ages. Relative quantitation was done using the expression at 3-dpp (days post-partum) as 1. Note that *Rpl39* expression decreased about 8-fold from 3-dpp to 8-WK, whereas *Rpl39l* expression increased about 90-fold during the same time of mouse development. *Gapdh* was used as the control. Images of agarose gel electrophoresis of RT-PCR products are shown below.

(C) Schematic drawing of *Rpl39l* genomic region. *Rpl39l* gene is located in chromosome 12 in mouse. It contains three exons, of which exon 3 encodes the 153-nt (nucleotide) long cDNA for the 51-amino acid long RPL39L protein. Positions of two sgRNAs are indicated. sgRNAs and Cas9 mRNA were injected into 2-cell mouse embryos, which were then transplanted into oviduct of pseudo-pregnant female mice. One newborn carried an insertion mutation that caused frame shift (Ins/FS). The resulting cDNA and predicted amino acid sequence are shown in red. An early stop codon is generated due to the frame shift mutation. This mutation was generated by sgRNA-1 near the start codon. Three amino acids (A2, Q28 and M36)

that are different from RPL39 are underlined. Primers for genotyping the mice are shown above.

(D) Genotyping of mice. Mutants contain a 19-nt insertion.

(E) RT-PCR of mouse testes. Total RNAs extracted from mice with different genotypes were reverse transcribed using oligo-dT, followed by PCR with gene specific primers. Mice homozygous to *Rpl39l* mutation expressed mRNAs 19-nt longer than that of wild type, whereas heterozygous mutant mice expressed both.

(F) Western blotting of mouse testes. The pan-anti-RPL39/RPL39L antibody recognized both RPL39 and RPL39L on Western blot. The decreased total RPL39/RPL39L level in testes from *Rpl39l*$^{-/-}$ mice suggests that RPL39L is likely absent.

(G) Immuno-staining of testis sections from 2-week old mice, using the antibody that recognizes both RPL39 and RPL39L. Decreased fluorescent signals from spermatogonial stem cells to spermatocytes in *Rpl39l*$^{-/-}$ mice are consistent with the deletion of RPL39L. Borders of cross-sections of seminiferous tubules are outlined by dashed white lines. Cell nuclei were stained with DAPI. Scale bar: 20 μm.

(H) Immuno-staining of testis sections from adult (3-month old) mice, using the antibody that recognizes both RPL39 and RPL39L. Decreased fluorescent signals in *Rpl39l*$^{-/-}$ mice are consistent with the deletion of RPL39L. Intense fluorescent signals were detected near the luminal area of seminiferous tubules (outlined in dashed yellow lines), where elongating spermatids and residue bodies are located.

Presumably mainly RPL39L is expressed at this late stage of spermatogenesis (see also S1B) and eliminated from mature sperm by residue bodies. However, little signal was detected in the same area in *Rpl39l*$^{-/-}$ mice, suggesting the absence of RPL39/RPL39L proteins. Cell nuclei were stained with DAPI. Scale bar: 20 μm.

Figure S2. Computer assisted sperm analysis (CASA). Related to Figure 1.

Various parameters were measured using SCA software from recordings of sperm samples. Total motility (A) and progressive motility (B) were decreased in *Rpl39l*$^{-/-}$ mice, whereas LIN (H), STR (I), WOB (J) and BCF (K) were slightly increased. N = 5, 5 and 4 mice for wild type, *Rpl39l*$^{+/-}$ and *Rpl39*$^{-/-}$ mutants, respectively, One-way ANOVA Tukey's test, $*P < 0.05$, $**P < 0.01$. VCL: curvilinear velocity; VSL: straight line velocity; VAP: average path velocity; ALH: amplitude of lateral head; LIN: linearity; STR: VAP/VSL straightness; WOB: wobble VAP/VCL; BCF: beat cross frequency.

Figure S3. Flow cytometry of mouse testicular cells. Related to Figure 2.

(A) Hematoxylin/Eosin staining of testis sections from 1-week old mice. Percent of spermatogenic cell populations shown on right. N = 6, 6 and 5 mice for wild type, *Rpl39l*$^{+/-}$ and *Rpl39*$^{-/-}$ mutants, respectively.

(B) Hematoxylin/Eosin staining of testis sections from 2-week old mice. Percent of spermatogenic cell populations shown on right. N = 5, 7 and 5 mice for wild type, *Rpl39l*$^{+/-}$ and *Rpl39*$^{-/-}$ mutants, respectively.

(C) Hematoxylin/Eosin staining of testis sections from 4-week old mice. Percent of spermatogenic cell populations shown on right. N = 5, 6 and 9 mice for wild type, *Rpl39l*$^{+/-}$ and *Rpl39*$^{-/-}$ mutants, respectively.

(D) Hematoxylin/Eosin staining of testis sections from 8-week old mice. Percent of spermatogenic cell populations shown on right. N = 6, 6 and 6 mice for wild type, *Rpl39l*$^{+/-}$ and *Rpl39*$^{-/-}$ mutants, respectively, no significant differences were found.

(E) Hematoxylin/Eosin staining of cauda epididymis from adult (3-month old) mice. See also Fig. 1F.

(F) Representative images of cell flow cytometry. Percentages of each cell populations are indicated in graphs. Cells were stained with Hoechst 33342.

(G) Percent of haploid spermatid populations in testes of 4-week old mice. N = 6, 6 (7 for G7) and 9 mice for wild type, *Rpl39l*$^{+/-}$ and *Rpl39*$^{-/-}$ mutants, respectively.

One-way ANOVA Tukey's test, $*P < 0.05$, $**P < 0.01$, $***P < 0.001$. For A-D and F-G: G1: spermatogonia, G2: diploid cells, G3: pre-leptotene to leptotene spermatocytes, G4: pachytene spermatocytes (4N), G5: MII spermatocytes, G6: haploid spermatids, G7: round spermatids and G8: elongating spermatids.

Figure S4. Meiotic cell cycle progression. Related to Figure 2.

(A) Percent of SYCP3^{+} spermatocytes-containing cross-sections in total testis cross-sections counted. Testis sections of 2-week old mice were stained with anti-SYCP3. N = 3 experimental repeats.

(B) Number of SYCP3^{+} spermatocytes in cross-sections of adult mouse testis. Sections were stained with anti-SYCP3. N ≥ 63 cross-sections.

(C) Immuno-staining of SYCP3 in adult testis cross-sections. Cell nuclei were stained with DAPI. Scale bar: 50 μm.

(D) Representative images of Giemsa staining of chromosomal spread. Mid-pachytene, MI (meiosis I metaphase) and MII (meiosis II metaphase) spermatocytes appeared similar in both wild type and *Rpl39l*$^{-/-}$ mice.

(E) Ratio of MMI and MMII spermatocytes. N = 4 experimental repeats, no significant differences were found.

(F) Number of metaphase cells in every 1000 mid-pachytene spermatocytes counted. N = 4 experimental repeats, no significant differences were found.

(G) Representative confocal images of immuno-staining of SYCP3 and γH2AX in chromosomal spread. Chromosome condensation and sex body formation appeared similar in wild type and *Rpl39l*$^{-/-}$ mice. Scale bars: 10 μm.

(H) Percent of spermatocytes at different stages of meiotic cell cycle. N = 3 experimental repeats, no significant differences were found.

One-way ANOVA Tukey's test, $*P < 0.05$, $**P < 0.01$, $***P < 0.001$.

Figure S5. Proliferating spermatogonial stem cells affected by *Rpl39l* deletion. Related to Figure 2.

(A) Representative confocal images of seminiferous tubules from 2-week old and adult (3-month old) mice immuno-stained with anti-GFRα1. Cell nuclei were stained with DAPI. Scale bar: 50 μm.

(B) Changes of SSC sub-populations in adult mice. While UCHL1^{+} spermatogonia (upper panel) and total PLZF^{+} SSCs showed no apparent differences (middle panel), the ratio of PLZF^{Low} to PLZF^{High} SSCs were decreased in *Rpl39l*$^{-/-}$ mice (lower panel) (N $\geq$ 75 cross-sections).

(C) Representative FACS graphs showing no changes of cKIT^{+} and cKIT^{-} cell populations in PLZF^{High} SSCs.

(D) Percent of PLZF^{High} SSCs that are either cKIT^{+} or cKIT^{-} in 2-week old mice. N $\geq$ 5 testes, paired-sample *t*-test, no significant differences were found.

(E) Representative confocal images of seminiferous tubules immuno-stained with anti-PLZF and anti-cKIT. Note that cKIT was expressed mostly in PLZF^{Low} SSCs. Scale bar: 50 μm.

(F) Apoptotic cells in mouse testes. TUNEL staining showed that both percent of TUNEL^{+} cross-sections (middle panel) and TUNEL^{+} cells per TUNEL^{+} cross-section increased in adult mice (right panel) (N $\geq$ 117 cross-sections). Although percent of TUNEL^{+} cross-sections did not change dramatically in 2-week old *Rpl39l*$^{-/-}$ mice (left panel) (N = 4, 5 and 5 testes for wild type, *Rpl39l*$^{+/-}$ and *Rpl39*$^{-/-}$ mice, respectively), number of TUNEL^{+} cells/ TUNEL^{+} cross-section was increased (see Figure 2J-K).

(G) Representative confocal images of testis sections immuno-stained with anti-SOX9. Cell nuclei were stained with DAPI. Scale bar: 50 μm.

(H) Number of Sertoli cells per cross-section of testes from 2-week old and adult mice with different genotypes. N ≥ 90 cross-sections, no significant differences were found.

One-way ANOVA Tukey's test, $*P < 0.05$, $**P < 0.01$, $***P < 0.001$.

Figure S6. GST pull-down of RPL39/RPL39L protein complexes and the effect of *Rpl39l* deletion on mitochondria proteins. Related to Figures 4 and 6.

(A) Representative confocal images of cross-sections immuno-stained with anti-RPL39/RPL9L and anti-γH2AX. In early spermatocytes where no sex body appears, RPL39/RPL39L are mainly localized in the nuclei of cells. With the sex body formation, spermatocytes enter pachytene stages of prophase, RPL39/RPL39L are more concentrated in cytoplasm of cells. Cell nuclei were stained with DAPI. Scale bar: 50 μm.

(B) Coomassie blue staining of GST pull-down samples. Control is GST transformed bacterial without IPTG induction.

(C) Western blotting of GST pull-down samples using anti-GST antibody. Control is GST transformed bacterial without IPTG induction.

(D) Venn diagram of proteins pulled-down by GST-RPL39 and GST-RPL39L, as identified by mass spectrometry. 190 and 164 proteins identified in protein

complexes pulled-down by GST-RPL39 and GST-RPL39L, respectively, after selection by unique peptides > 3, protein sequence coverage > 20% and iBAQ intensity > 100000. Among them, about 66% of proteins overlapped.

(E) GO analysis of the common proteins pulled-down by both GST-RPL39 and GST-RPL39L. Proteins are enriched with functional roles in ribosome biogenesis, RNA binding and processing (blue) and ubiquitin conjugation (yellow). Many of them are associated with ribosome biogenesis and nucleus (green) and may be modified by post-translational modifications.

(F) Western blotting of sub-cellular fractionations. LAMIN B1, α-TUBULIN and COXIV were used as markers for nucleus, cytoplasm and mitochondria. N: nucleus, C: cytoplasm and M: mitochondria.

(G) Heatmap of mitochondrial proteins identified by mass spectrometry. Three experimental repeats were highly repeatable. 72 and 62 proteins were found to either down-regulated or up-regulated in *Rpl39l*$^{-/-}$ mice, respectively. DEPs are clustered into five clusters according to their similarities in changes. Red: upregulated DEPs, Blue: downregulated DEPs.

(H) Volcano plot of differentially expressed proteins identified from mitochondrial fractions isolated from wild type and *Rpl39l*$^{-/-}$ mice. Known mitochondria-specific proteins are indicated in red, whereas others associated with multiple organelles are indicated in orange.

Figure S7. Degenerative spermatogenesis in aging mice. Related to Figure 7.

(A) Hematoxylin/Eosin staining of testis sections from 8-month old mice.

(B) Body weight of mice at 8-month of age. N = 5 mice for each genotype, no significant differences were found.

(C) Testis weight of mice at 8-month of age. N = 5 testes for each genotype.

(D) Percent seminiferous tubules with degenerative spermatogenesis at 8-month of age. N = 4 testes for each genotype.

(E) Numbers of sperm obtained from cauda epididymides of 8-month old mice. N = 5 (4 for wild type) epididymides for each genotype.

(F) Percent motile sperm obtained from cauda epididymides of 8-month old mice. N = 5 (4 for wild type) epididymides for each genotype.

One-way ANOVA Tukey's test, $*P < 0.05$, $**P < 0.01$, $***P < 0.001$.